JCI insight

RESEARCH ARTICLE

Carbon monoxide–induced metabolic switch in adipocytes improves insulin resistance in obese mice

Laura Braud,[1,2] Maria Pini,[2,3] Lucie Muchova,[4] Sylvie Manin,[1,2] Hiroaki Kitagishi,[5] Daigo Sawaki,[2,3] Gabor Czibik,[2,3] Julien Ternacle,[2,3] Geneviève Derumeaux,[2,3] Roberta Foresti,[1,2] and Roberto Motterlini[1,2]

[1]Inserm U955, Team 12, Créteil, France. [2]Faculty of Medicine, University Paris-Est, Créteil, France. [3]Inserm U955, Team 8, Créteil, France. [4]Institute of Medical Biochemistry and Laboratory Diagnostics, First Faculty of Medicine, Charles University, Prague, Czech Republic. [5]Department of Molecular Chemistry and Biochemistry, Faculty of Science and Engineering, Doshisha University, Kyotanabe, Kyoto, Japan.

Obesity is characterized by accumulation of adipose tissue and is one the most important risk factors in the development of insulin resistance. Carbon monoxide–releasing (CO-releasing) molecules (CO-RMs) have been reported to improve the metabolic profile of obese mice, but the underlying mechanism remains poorly defined. Here, we show that oral administration of CORM-401 to obese mice fed a high-fat diet (HFD) resulted in a significant reduction in body weight gain, accompanied by a marked improvement in glucose homeostasis. We further unmasked an action we believe to be novel, by which CO accumulates in visceral adipose tissue and uncouples mitochondrial respiration in adipocytes, ultimately leading to a concomitant switch toward glycolysis. This was accompanied by enhanced systemic and adipose tissue insulin sensitivity, as indicated by a lower blood glucose and increased Akt phosphorylation. Our findings indicate that the transient uncoupling activity of CO elicited by repetitive administration of CORM-401 is associated with lower weight gain and increased insulin sensitivity during HFD. Thus, prototypic compounds that release CO could be investigated for developing promising insulin-sensitizing agents.

Introduction

Obesity is one the most important risk factors leading to metabolic dysfunction and type 2 diabetes (1). Excessive accumulation of visceral fat is accompanied by chronic low-grade inflammation, contributing to the development of insulin resistance, hyperglycemia, and adipose tissue dysfunction (2, 3). Whether malfunction of mitochondria, which play a crucial role in cellular bioenergetics, is implicated in adipose tissue dysfunction is still debated (4). Indeed, defective mitochondrial activity can lead to impaired fatty acid oxidation and glycolysis, thereby causing disruption of lipid and glucose metabolism (4). It has also been reported that mitochondrial oxidative stress in adipocytes diminishes insulin-stimulated GLUT4 translocation and glucose uptake, resulting in insulin resistance (5). In contrast, an increased glucose tolerance and insulin sensitivity was observed in mice with genetically altered mitochondrial oxidative phosphorylation (6), and an enhanced mitochondrial capacity was described in human subjects with insulin resistance (7). Nevertheless, pharmacological interventions that target mitochondria for the treatment of diabetes have attracted a strong interest over the last decade (8, 9). For example, mitochondrial uncoupling agents, such as 2,4-dinitrophenol or niclosamide ethanolamine, have demonstrated promising effects on diabetic symptoms in mice by both promoting substrate oxidation and reducing oxidative stress in mitochondria (10, 11).

Emerging evidence indicates that carbon monoxide (CO) modulates metabolism in different cell types (12–15). CO is a ubiquitous gaseous molecule produced in mammalian cells and tissues through the breakdown of heme catalyzed by heme oxygenase (HO) enzymes (16). Initially considered to be a toxic product, CO is now recognized as a key signaling molecule with vasoactive and cardioprotective effects as well as antithrombotic, antiapoptotic and antiinflammatory properties (17, 18). In relation to cellular metabolism, we have shown that small amounts of CO increase O_2 consumption in cells via a mild uncoupling activity

Conflict of interest: The authors have declared that no conflict of interest exists.

Submitted: July 12, 2018
Accepted: October 16, 2018
Published: November 15, 2018

Reference information:
JCI Insight. 2018;3(22):e123485.
https://doi.org/10.1172/jci.insight.123485.

in mitochondria that is accompanied by changes in the production of reactive oxygen species (12). The use of CO-releasing molecules (CO-RMs), a class of compounds that release controlled quantities of CO into cells and tissues, has helped to unravel this novel mechanism of action and identify the potential therapeutic effects of this gas (12, 17, 19, 20). Accordingly, the water-soluble CORM-A1 has been shown to improve dietary-induced obesity, hyperglycemia, and insulin resistance in mice (21, 22). However, the mechanisms underlying this beneficial outcome of CO in obesity have been poorly investigated.

In the current study, we examined the effect of CORM-401 on whole-body insulin sensitivity and glucose tolerance in C57BL6 mice subjected to an obesogenic high-fat diet (HFD). We report that oral administration of CORM-401 reduces the gain in body weight and improves insulin resistance in HFD-fed obese mice. CO delivered by CORM-401 to adipose tissue and cells uncouples mitochondrial respiration, leading to an increase in glycolysis to maintain ATP levels. This metabolic switch was associated with higher phosphorylation of the insulin signaling effector Akt and was accompanied by an amelioration of systemic and adipocyte insulin sensitivity. Our data demonstrate that the effect of CO on cellular bioenergetics in adipose tissue serves to counteract insulin resistance in obese mice.

Results

Oral administration of CORM-401 reduces body weight gain and improves insulin resistance in HFD-induced obesity in mice. We have shown recently that CORM-401, a manganese-based compound that releases 3 equivalents of CO/mol (structure shown in Supplemental Table 1; supplemental material available online with this article; https://doi.org/10.1172/jci.insight.123485DS1), exerts a stronger vasodilatory effect and angiogenic activity than CORM-A1, a boron compound that liberates only 1 CO/mol (20). Thus, it appears that CORM-401 exhibits enhanced pharmacological activities due to liberation of higher amounts of CO. Since CORM-401 has never been tested in vivo, we first determined the levels of blood carbonmonoxy hemoglobin (COHb) in mice receiving CORM-401 at 2 different doses after oral gavage. Figure 1A and Supplemental Figure 1A show that COHb significantly increased to 2.5% and 4.5% 30 minutes after administration of CORM-401 at 15 and 30 mg/kg, respectively, and gradually decreased to control levels over a period of 48 hours. These data confirm that CO is released by CORM-401 and delivered into the circulation in a dose-dependent fashion. Based on this kinetic, we decided to assess the metabolic effects of CORM-401 (15 and 30 mg/kg) administered 3 times a week to mice fed either a standard diet (SD) or a HFD for 14 weeks. As shown in Supplemental Figure 1, B–E, CORM-401 decreased body weight gain and improved both glucose metabolism and insulin resistance in a dose-dependent manner in HFD-fed mice, but the effect was significant only at the dose of 30 mg/kg. Because consistent results were obtained with 30 mg/kg CORM-401, we decided to continue our investigation using this dose in two distinct protocols whereby CORM-401 was given in concomitance with the HFD (prevention group, HFD + CORM-P) or 6 weeks after beginning the HFD (treatment group, HFD + CORM-T). Body weight gain was significantly increased by the HFD and was reduced by CORM-401 in both the prevention and the treatment group (Figure 1, B and C), as reflected by decreased plasma leptin (Figure 1M). Changes in body weight were not due to differences in food intake between the groups (Table 1). In addition, mice fed with SD and SD plus CORM-401 displayed similar body weight, suggesting that the compound was well tolerated and the reduced weight gain in HFD-fed mice was not due to a toxic effect of the drug (Supplemental Figure 2, A and B). In addition, we did not observe any change in cardiac function parameters by CORM-401 compared with untreated obese mice (Supplemental Table 2). Interestingly, CORM-401 did not affect glucose metabolism in SD-fed mice (Supplemental Figure 2, C–F) but improved whole-body glucose tolerance and insulin sensitivity in HFD-fed mice, as shown by a significant decrease in glycemia (Figure 1, D–G). In line with this, CORM-401 decreased fasting plasma glycemia and insulin, improving the calculated HOMA-IR in HFD-fed mice (Figure 1, J–L), while plasma cholesterol and triglyceride levels remained unchanged (Figure 1, H and I). These results indicate that CORM-401 counteracts body weight gain, impaired glucose tolerance, and insulin resistance induced by HFD in mice.

CORM-401 remodels adipose tissue in obese mice. We next investigated the effect of CORM-401 on adipose tissue metabolic and inflammatory profiles. Even though epididymal white adipose tissue (eWAT) weight was not affected by CORM-401 (Figure 2, A and B), the size of adipocytes was significantly reduced by 25% in the HFD + CORM-P group (Figure 2, A and C). Interestingly, conditioned media of eWAT collected from both mice groups administered with CORM-401 displayed lower nonesterified free fatty acid content compared with that in the HFD group (Figure 2D). Furthermore, the mRNA expression of the key metabolic genes *PPar-γ*, adiponectin, *Fabp4*, *Hsl*, *Glut4*, *Irs1*, *Hk2*, and *Vegf* was decreased by the HFD (Figure 2E) and restored

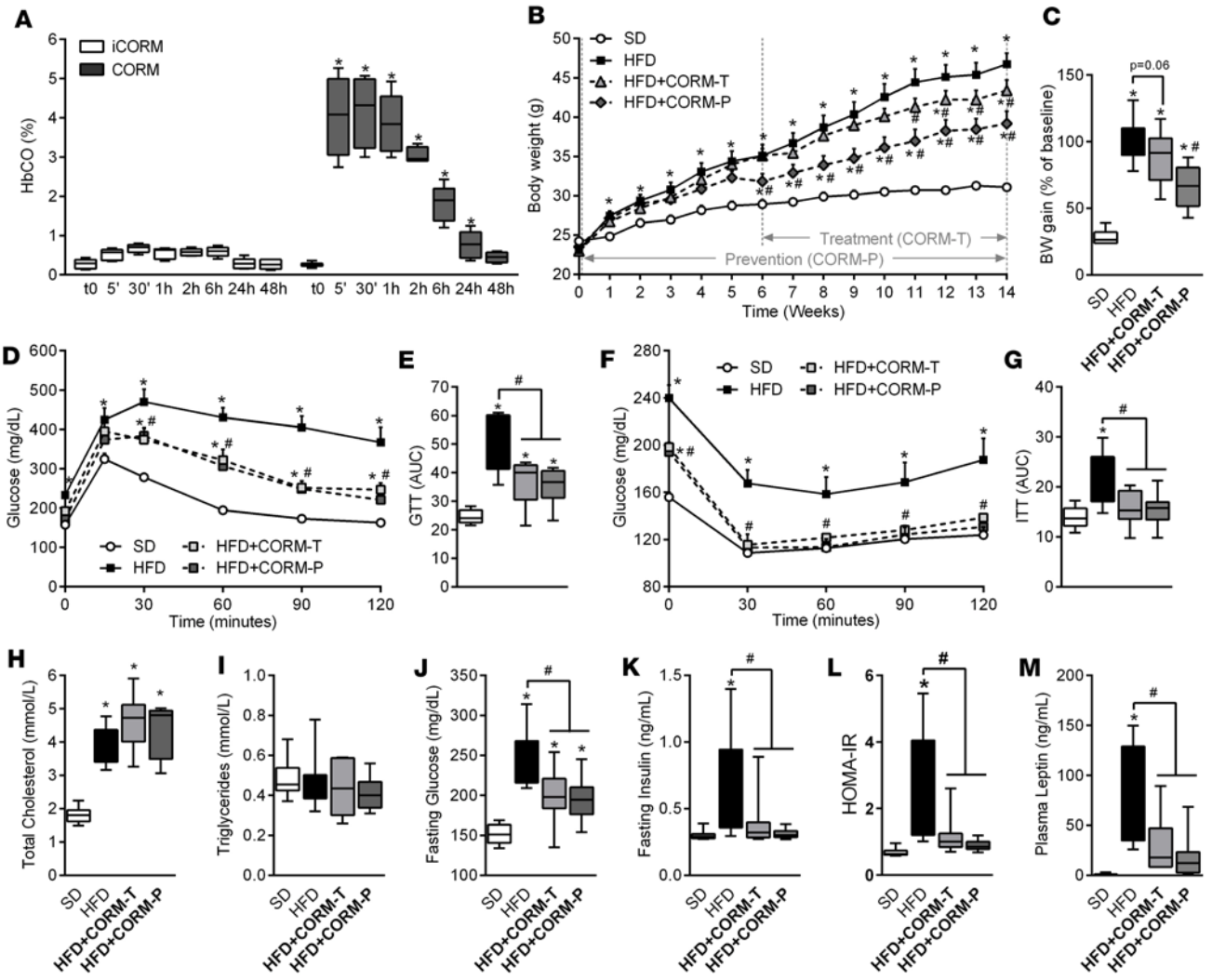

Figure 1. CORM-401 reduces body weight gain and improves insulin resistance in high-fat diet–induced obesity. Mice received a standard diet (SD) or high-fat diet (HFD) for 14 weeks. CORM-401 (30 mg/kg) was given by oral gavage starting either at the beginning of (HFD + CORM-T) or after 6 weeks of (HFD + CORM-P) HFD. Carbonmonoxy hemoglobin (COHb) was measured after oral gavage with CORM-401 (**A**). Body weight (BW) was measured every week (**B**) and BW gain was calculated as the percentage of the basal weight (**C**). A glucose tolerance test (GTT) was performed at week 13 (**D**), and data represent the area under the curve (GTT AUC) (**E**). An insulin tolerance test (ITT) was performed at week 14 (**F**), and data represent the area under the curve (ITT AUC) (**G**). Fasting total cholesterol (**H**), fasting triglycerides (**I**), fasting glucose (**J**), fasting insulin (**K**), calculated HOMA-IR (**L**), and fasting leptin (**M**) were measured after 14 weeks in all groups examined. Values represent the mean ± SEM. n = 4–6 mice per group (**A**); n = 8–10 mice per group (**B**–**M**). $^{*}P <$ 0.05 vs. control group (SD), $^{\#}P < 0.05$ vs. HFD group, values not designated with symbols are not statistically different, Student's t test or 1-way or 2-way ANOVA with Fisher multiple comparison test.

to basal levels by CORM-401 in the HFD + CORM-P group but not in HFD + CORM-T group. In contrast, mRNA expression of *PPar-α*, *Pgc1-α*, and *Cpt1* was decreased by HFD but remained unchanged after CORM-401 treatment (data not shown). Significant remodeling in other fat pads, particularly in brown adipose tissue (BAT), was evident in the reduction of weight and lipid content in both groups administered with CORM-401 (Supplemental Figure 3, A–E). Similarly to that in eWAT, mRNA expression of the metabolic genes *PPar-γ*, *Vegf*, adiponectin, *Pgc1-α*, and *Ucp1* was decreased in BAT of HFD-fed obese mice and fully or partially restored in the HFD + CORM-P group (Supplemental Figure 3G). Conversely, gene expression of metabolic markers in subcutaneous adipose tissue was not affected by CORM-401 (Supplemental Figure 3F). Despite the fact that HFD did not induce a high-grade inflammation in our model, CORM-401 still modulated local inflammation in obese mice. First, the increased macrophage infiltration induced by HFD was virtually abolished by CORM-401 administration (Figure 2, F and G), although the induction of *Ccl2* was unchanged by the compound (Figure 2H). Second, CORM-401 decreased *Hmox-1* expression induced by HFD (Figure 2I)

Table 1. Food intake

Food intake (g/mouse/d)	SD	HFD	HFD + CORM-T	HFD + CORM-P
4th week	3.8 ± 0.2	2.8 ± 0.2[A]	2.8 ± 0.2[A]	2.6 ± 0.3[A]
8th week	3.6 ± 0.1	3.1 ± 0.1[A]	3.0 ± 0.2[A]	2.7 ± 0.1[A]

Results are shown as mean ± SEM. [A]Significantly different compared with values in the same time period (before treatment or during treatment). $P < 0.05$, 1-way ANOVA with Fisher multiple comparison test.

and the levels of IL-6, IL-1β, and IL-10 in eWAT-conditioned media (Figure 2J). These data demonstrate that the positive effects of CORM-401 on weight gain and metabolism in obese mice correlate with an amelioration of adipose tissue structure, function, and inflammation.

CORM-401 had no effect on the liver, another crucial organ for the maintenance of glucose homeostasis. In fact, CORM-401 did not modify the increase in liver weight (1.5-fold) and lipid content caused by HFD (Supplemental Figure 4, A–C) and only marginally affected the deregulation of the metabolic genes *PPar-γ*, *Hk2*, *Irs1*, *Hsl*, and *Fabp4* induced by HFD (Supplemental Figure 4D). We note that the plasmatic indexes of liver injury were not affected by HFD (Table 2), suggesting nonadvanced hepatic steatosis without major injuries.

CO delivered by CORM-401 increases systemic and adipocytes insulin sensitivity. To elucidate whether the improved insulin resistance promoted by CORM-401 is linked to an effect of CO on adipocytes, we assessed insulin sensitivity in eWAT and 3T3-L1 adipocytes. We first confirmed that CO content in eWAT increased significantly 2 and 6 hours after oral gavage with CORM-401 compared with eWAT from mice treated with PBS or inactive CORM-401 (iCORM) (Figure 3A). We then determined glucose levels in mice treated with PBS, iCORM, or CORM-401 1 hour prior to intraperitoneal injection of insulin (Figure 3B) and showed that only CORM-401 enhanced systemic insulin sensitivity (Figure 3, C and D). In addition, phosphorylation of protein kinase B (Akt) induced by insulin was increased in eWAT from CORM-401–treated mice compared with control mice (Figure 3, E and F). This response was recapitulated in eWAT of obese mice following oral gavage with CORM-401 (Supplemental Figure 5). As observed in eWAT, CO content in 3T3-L1 adipocytes exposed to 50 μM CORM-401 was significantly higher compared with that in cells treated with PBS or iCORM (Figure 3G). Likewise, only CORM-401–treated adipocytes exhibited increased Akt phosphorylation in basal conditions and after stimulation with insulin (20 nM) for 10 minutes (Figure 3, H–J). These data demonstrate that CO liberated from CORM-401 accumulates in adipose tissue and regulates Akt signaling to improve insulin sensitivity.

CO uncouples mitochondrial respiration and increases glycolytic rate in adipocytes. We next investigated the effects of CORM-401 on adipocyte bioenergetics based on the emerging evidence that CO is a metabolic regulator in vascular, inflammatory, and cancer cells (12, 23). Using MitoStress assays, we showed that CORM-401–treated 3T3-L1 adipocytes display a concentration-dependent increase in oxygen consumption rate (OCR), even in the presence of the ATP synthase inhibitor oligomycin (Figure 4A and Supplemental Figure 6), resulting in decreased ATP-linked respiration (or coupled respiration) and higher proton leak (or uncoupled respiration) compared with untreated cells (Figure 4B). This effect was followed by reduced respiration in response to the uncoupling agent FCCP and augmented nonmitochondrial respiration after addition of rotenone/antimycin A. These results indicate an uncoupling activity of CORM-401 in adipocytes, as previously observed in other cell types (12). Interestingly, in the absence of inhibitors of the electron transport chain, CORM-401 induced a transient increase in OCR lasting for 2 to 3 hours, depending on the dose used. This effect was concomitant with a rise in glycolysis, as assessed by the extracellular acidification rate (ECAR) (Figure 4, C and D). Accordingly, intracellular lactate was increased by CORM-401 (Figure 4E). A glycolysis stress test confirmed that CORM-401, but not iCORM, enhanced ECAR in adipocytes following sequential addition of glucose, oligomycin, and 2-DG (Figure 4, F and G). Increased glycolysis was not an artifact due to acidification of the medium by CORM-401, since blocking this pathway with 2-DG completely prevented the effects of CORM-401.

Notably, intracellular ATP levels were higher in CORM-401–treated adipocytes compared with iCORM-treated adipocytes, suggesting that glycolysis is engaged as a compensatory mechanism for maintenance of energy (Figure 4H). ATP content was diminished by 2-DG in iCORM- and CORM-401–treated cells; however, this decrease was more pronounced in adipocytes exposed to CORM-401, likely a result

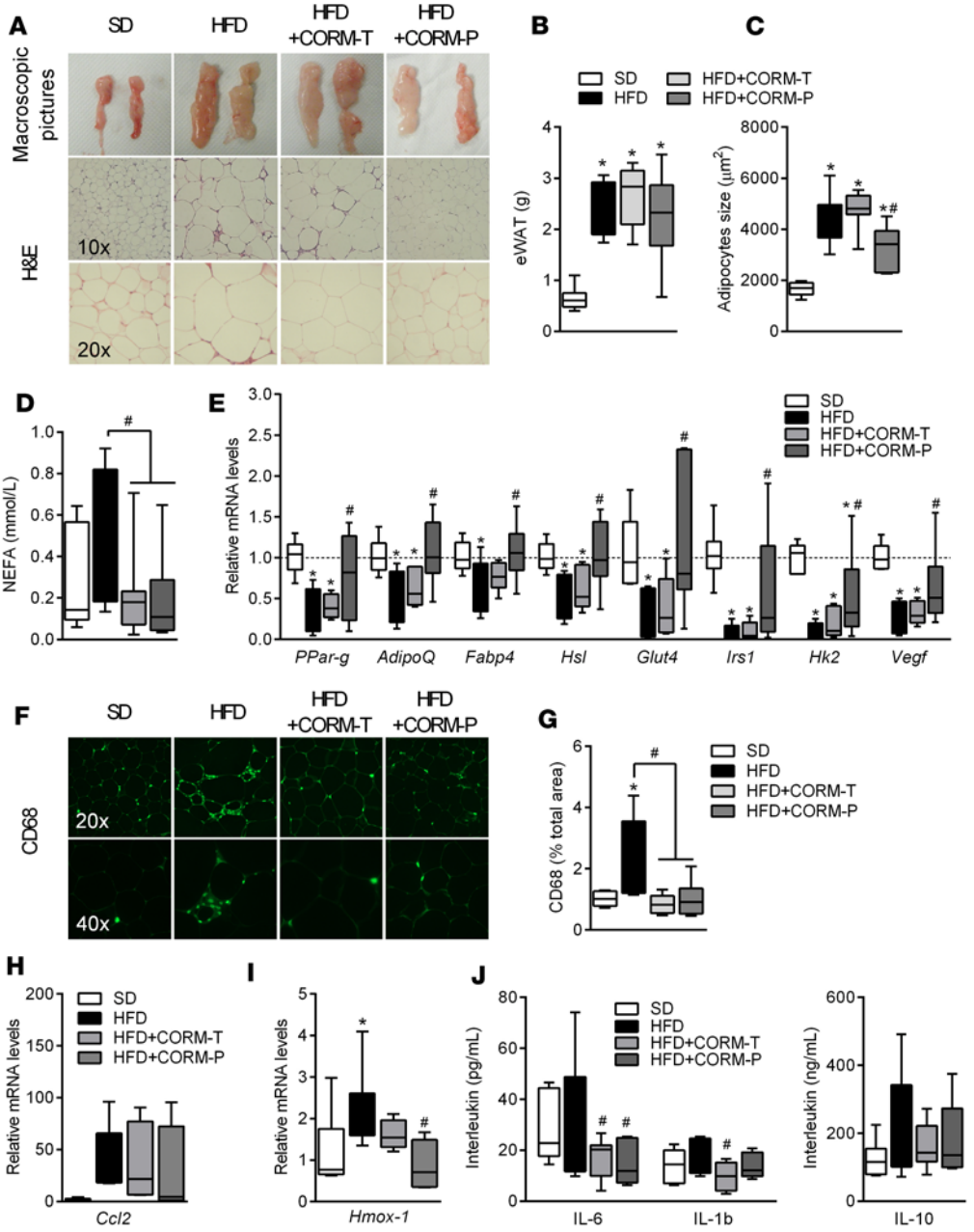

Figure 2. CORM-401 improves visceral adipose tissue function in HFD-induced obesity. Mice on standard (SD) or high-fat diet (HFD) were sacrificed after 14 weeks. CORM-401 (30 mg/kg) was given by oral gavage starting either at the beginning (HFD + CORM-T) or after 6 weeks (HFD + CORM-P) HFD. Images and representative sections of epididymal white adipose tissue (eWAT) stained with H&E (**A**). eWAT was also evaluated for weight (**B**), adipocyte size (**C**), free fatty acids levels from conditioned media (**D**), mRNA expression of genes involved in metabolism (**E**), CD68 expression (**F** and **G**), and mRNA expression of *CCl2* (**H**) and *Hmox-1* (**I**) as well as interleukin content from conditioned media (**J**). mRNA expression was determined by real-time PCR and normalized to β-actin. Values represent the mean ± SEM. n = 6–8 mice/group. $^{*}P < 0.05$ vs. control group (SD), $^{\#}P < 0.05$ vs. HFD group, 1-way ANOVA with Fisher multiple comparison test. Values not designated with symbols are not statistically different.

of the uncoupling effect of CO and the inhibition of respiration caused by CORM-401 at the end of the experiment (Figure 4H). We wanted to verify whether this metabolic switch induced by CORM-401 occurs in vivo by assessing OCR and ECAR in eWAT collected from mice treated with iCORM or CORM-401 (Figure 4I). Although no significant differences were observed in basal OCR between the two groups, the response to FCCP was lower after treatment with CORM-401 (Figure 4J), as shown in cultured adipocytes. Most importantly, ECAR was also higher in eWAT punches from CORM-401–treated mice (Figure 4K)

Table 2. Blood analysis

	SD	HFD	HFD + CORM-T	HFD + CORM-P
ASAT/ALAT	3.0 ± 0.5	2.5 ± 0.9	3.6 ± 0.9	2.9 ± 0.7
Conjugated bilirubin (μmol/l)	0.62 ± 0.2	0.47 ± 0.07	0.46 ± 0.06	0.36 ± 0.03
Total bilirubin (μmol/l)	6.46 ± 2.1	4.8 ± 2.1	7.4 ± 2.2	4.82 ± 1.9
Creatinine (mmol/l)	8 ± 0.8	10.13 ± 1.8	8.37 ± 1.0	7.43 ± 1.5
Lactate deshydrogenase (U/l)	191.2 ± 56.3	248.1 ± 46.5	321.3 ± 93.8	238 ± 66.3

ALAT, aspartate amino transferase; ASAT, alanine amino transferase. Results are shown as mean ± SEM. $P < 0.05$, 1-way ANOVA with Fisher multiple comparison test.

and lactate levels in conditioned medium from eWAT collected from mice receiving CORM-401 were increased (Figure 4L), confirming stimulation of glycolysis by CO in vivo.

ATP counteracts CO induced–metabolic switch in adipocytes and reverses CO-induced increase in insulin sensitivity. Our data indicate that CO induces a metabolic switch, favoring glycolysis, in adipocytes both in vitro and in vivo. If CO decreases mitochondrial ATP production because of transient uncoupling and/or partial inhibition of respiration leading to increased glycolysis to maintain ATP levels, we postulated that ATP per se could serve as the molecular trigger of this metabolic switch. To investigate this hypothesis, we artificially delivered ATP packaged in liposomes to adipocytes and examined the effects of CO on bioenergetics. ATP levels significantly increased in adipocytes after exposure to encapsulated ATP (Figure 5A). Importantly, exogenous ATP supplementation counteracted the rise in ECAR as well as lactate elicited by CORM-401 without affecting the increase in OCR (Figure 5, B–D). Furthermore, ATP delivery to adipocytes reversed the increase in insulin-dependent Akt phosphorylation induced by CO (Figure 5, E and F). Thus, the suppression of ECAR and Akt phosphorylation by ATP suggests that the increase in glycolysis by CO is a consequence of the uncoupling action of CO and is directly implicated in the improved insulin sensitivity observed in adipocytes.

Discussion

We report in this study that treatment with the CO-releasing agent CORM-401 decreases gains in body weight and markedly ameliorates glucose tolerance and insulin resistance in HFD-induced obese mice. We show that this effect is associated with prevention of adipose tissue alterations, as indicated by restoration in metabolic gene expression, suppression of macrophage infiltration, and reduction in key inflammatory markers (IL-6, IL-1β, and HO-1) characteristic of obesity. From a mechanistic point of view, we further show that CORM-401 (a) increases insulin sensitivity in adipose tissue by activation of Akt phosphorylation and (b) triggers a metabolic switch that is dependent on mitochondrial uncoupling by CO and is accompanied by an increase in glycolysis and lactate production. These results reveal an important role of CO in regulating bioenergetic metabolism in adipose tissue, thus counteracting the deleterious consequences of obesity.

We observed that administration of CORM-401 for the whole duration of HFD (CORM-P) was more effective in reducing body weight gain than treatment with CORM-401 starting 6 weeks after the beginning of the HDF regime (CORM-T). This effect is most likely due to a longer period of exposure to CO, since we noticed that a significant decrease in body weight becomes apparent in both groups 6 weeks after the first administration of CORM-401. Despite these differences, both groups exhibited the same improvement in glucose tolerance and insulin resistance, suggesting that the effect of CORM-401 on body weight is not the only factor explaining a beneficial role of CO on obesity-induced metabolic dysfunction. Indeed, a lower glycemia and increased insulin sensitivity were also found after one single administration of CORM-401 in lean mice, corroborating a direct pharmacological action of CO on glucose metabolism. When we focused on visceral adipose tissue (eWAT), which undergoes significant structural and functional changes during obesity, we also observed some interesting differences. Although CORM-401 did not affect the increased weight of eWAT in HFD-fed mice, a significant reduction in the size of adipocytes and a restoration of metabolic gene expression were evident in the CORM-P group. These effects correlate with the more pronounced decrease in weight gain in this group. However, both the CORM-P and CORM-T groups displayed a similar reduction in the secretion of nonesterified fatty acid, infiltration of macrophages, and

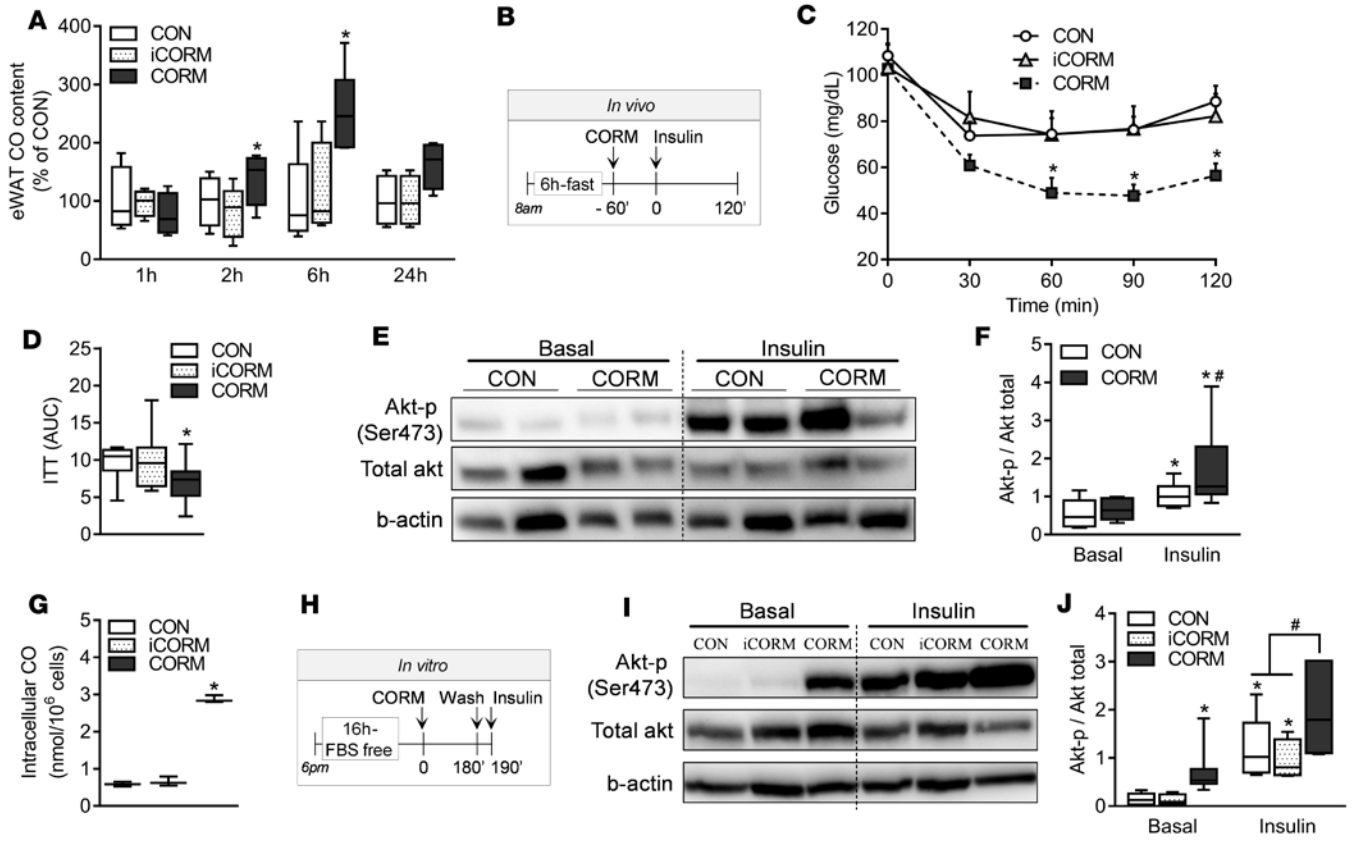

Figure 3. CO delivered by CORM-401 increases systemic and adipocytes insulin sensitivity both in vivo and in vitro. CO content was measured in epididymal white adipose tissue (eWAT) after oral gavage with PBS (CON), inactive CORM that does not release CO (iCORM, 30 mg/kg), or CORM-401 (30 mg/kg) (**A**). An ITT was performed in fasted mice 1 hour after oral gavage with PBS (CON), iCORM (30 mg/kg), or CORM-401 (30 mg/kg) (**B**), while blood glucose levels were measured at the times indicated (**C**) and represented by area under the curve (ITT AUC) (**D**). eWAT was evaluated for protein expression of total Akt and phosphorylated Akt assessed by Western blot (**E** and **F**). Intracellular CO level in 3T3-L1 adipocytes after CORM-401 exposure at 50 μM for 3 hours (**G**). Proteins were extracted from quiescent 3T3-L1 adipocytes after 3 hours exposure to PBS (CON), iCORM (50 μM), or CORM-401 (50 μM) (see protocol in **H**). Expression of total Akt and phosphorylated Akt was assessed by Western blot (**I** and **J**). Results are expressed as mean ± SEM. n = 4–6 mice per group (**A**); n = 10 mice per group (**C** and **D**); n = 8 mice per group (**E** and **F**); n = 3 in triplicates (**G**); n = 6 (**I**); n = 4 independent experiments (**J**). $^{*}P < 0.05$ vs. control group (CON), $^{\#}P < 0.05$ vs. insulin, 1-way ANOVA with Fisher multiple comparison test. Values not designated with symbols are not statistically different.

production of the proinflammatory cytokine IL-6 in eWAT, supporting the idea that the pharmacological action mediated by CO on these markers is also independent of the decrease in body weight gain. In particular, inhibition of macrophage infiltration and the marked suppression of IL-6, a cytokine strongly implicated in development of metabolic dysfunction during obesity (24, 25), indicate another potential mechanism by which CORM-401 exerts its beneficial effect on adipose tissue and insulin resistance. We also observed that treatment with CORM-401 diminishes HO-1 gene induction caused by HFD in adipose tissue. This is in line with previous studies showing that HO-1 is increased during HFD in mice (21) and humans (26). HO-1 upregulation in adipose tissue may be part of the adaptive response mounted by the organism to counteract the inflammatory and metabolic stress elicited by HFD. In fact, systemic induction of HO-1 by cobalt protoporphyrin or genetic overexpression of HO-1 reduces adiposity and improves insulin sensitivity in mice (27–30). However, the role of HO-1 in specific organs involved in metabolic regulation is still controversial, since it has also been reported that macrophage and hepatic HO-1 deletion protect against insulin resistance and inflammation (26, 31). Notably, in our study, we found that CORM-401 does not have any major effect on the liver. Thus, despite the fact that the liver is a crucial organ for the maintenance of glucose, the findings of this study strongly suggest that the beneficial effect of CO on glucose metabolism is mainly driven by its interaction with adipose tissue.

Our results confirm previous findings showing that CORM-A1, another CO-releasing agent, significantly diminishes body weight gain and insulin resistance when given intraperitoneally to HFD-fed mice

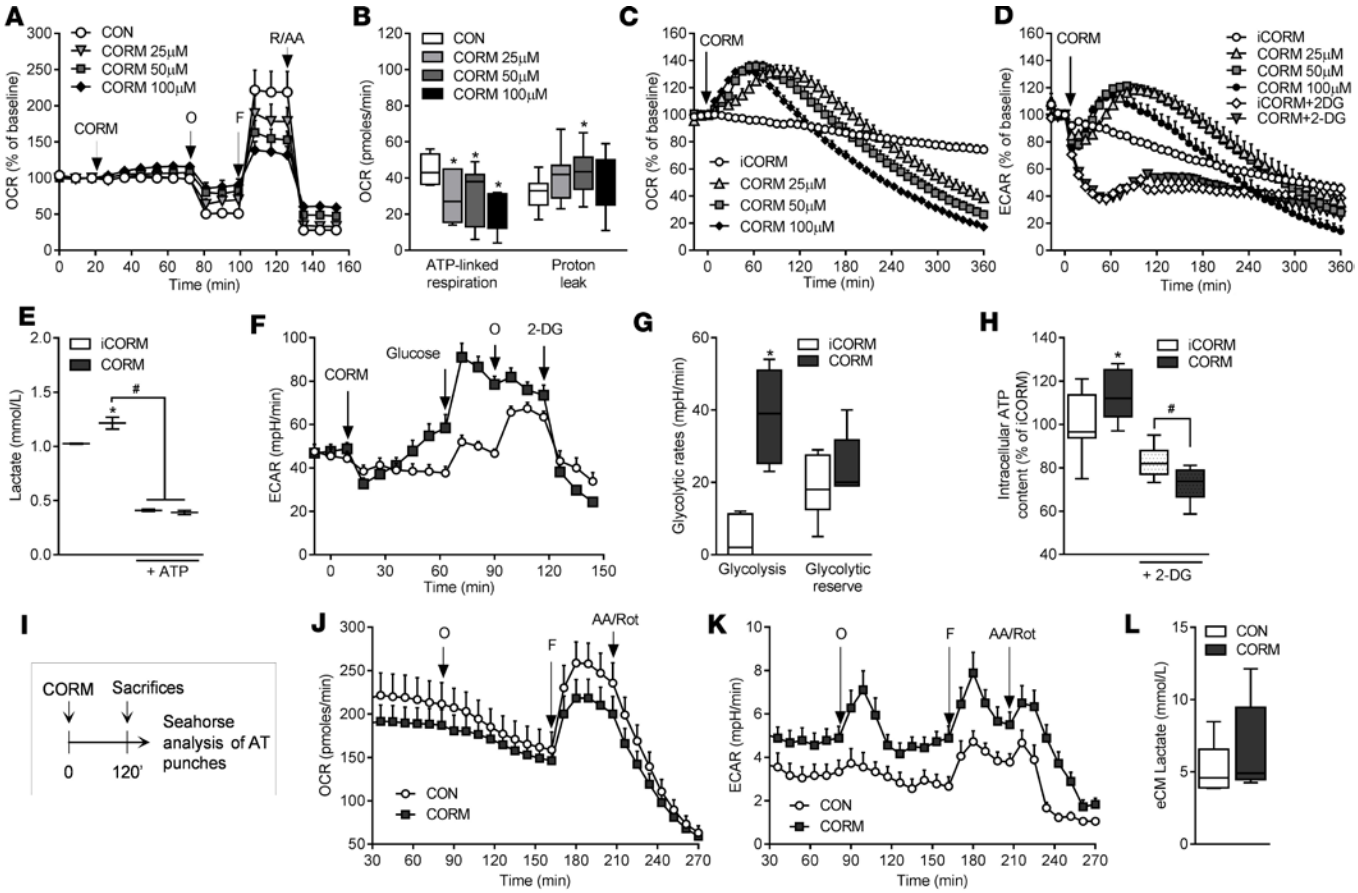

Figure 4. CO induces a metabolic switch in adipocytes in vitro and in vivo. Oxygen consumption rate (OCR) and extracellular acidification rate (ECAR) were measured in 3T3-L1 cells after addition of PBS (CON) or CORM-401 (25, 50, 100 μM). A MitoStress assay was performed on 3T3-L1 adipocytes after first addition of PBS or CORM-401, followed by sequential addition of oligomycin, FCCP, and rotenone/antimycin A (**A**). ATP-linked respiration rate was calculated by subtracting OCR values after oligomycin addition from basal OCR values, and proton leak was calculated by subtracting OCR values after R/AA addition from OCR values after oligomycin addition (**B**). OCR (**C**) and ECAR (**D**) were measured for 6 hours after addition of CORM-401. Lactate (**E**) and intracellular ATP (**H**) were measured 3 hours after exposure to iCORM or CORM-401 with or without 2-deoxyglucose (2-DG). A glycolytic assay was performed after addition of iCORM or CORM-401 (50 μM) followed by sequential addition of glucose, oligomycin, and 2-DG (**F**). Glycolysis rate was calculated by subtracting ECAR values after glucose addition from basal ECAR values, and glycolytic reserve was calculated by subtracting ECAR values after oligomycin addition from basal ECAR values (**G**). Experiments using the Seahorse Analyzer were performed on punches of eWAT collected from mice 2 hours after oral gavage with iCORM or CORM-401 (30 mg/kg) (see protocol in **I**), and OCR (**J**) and ECAR (**K**) were measured. Lactate was measured in eWAT-conditioned media (**L**). Results are expressed as mean ± SEM. $n = 4$ independent experiments (**A**–**D** and **F**–**H**); $n = 3$ independent experiments (**C**); $n = 6$ mice per group (**J**–**L**). $^{*}P < 0.05$ vs. control group (CON), $^{\#}P < 0.05$ vs. 2-DG, Student's t test or 1-way ANOVA with Fisher multiple comparison test. Values not designated with symbols are not statistically different.

for 30 weeks (17). A difference in our study is that CORM-401 was administered orally to mice. In addition, we advance the current knowledge on the pharmacological properties of CO-RMs by reporting that a transient increase in COHb levels is associated with accumulation of CO within the adipose tissue. Thus, we demonstrate that CO reaches the adipose tissue and modulates its function in vivo. This finding is further supported by the complete lack of effects by iCORM, which is depleted of CO. Importantly, we identified that CO directly affects insulin sensitivity, since phosphorylation of Akt, a major pathway implicated in insulin signaling, is significantly enhanced in adipocytes and adipose tissue after CORM-401 treatment. Despite the fact that increased Akt phosphorylation by CO has been reported in other cell types and tissues (32–34), the specific activation of this signal transduction pathway in adipose tissue likely explains the effect of CO on glucose metabolism independently from the reduction in weight gain.

The additional mechanism that most likely accounts for an improved glucose tolerance is the switch of adipose tissue metabolism toward glycolysis mediated by CO. This effect was confirmed by increased lactate production in adipocytes and in the secretome of adipose tissue after exposure to CORM-401, suggesting augmented glucose utilization. This metabolic switch occurred in concomitance with a rise in

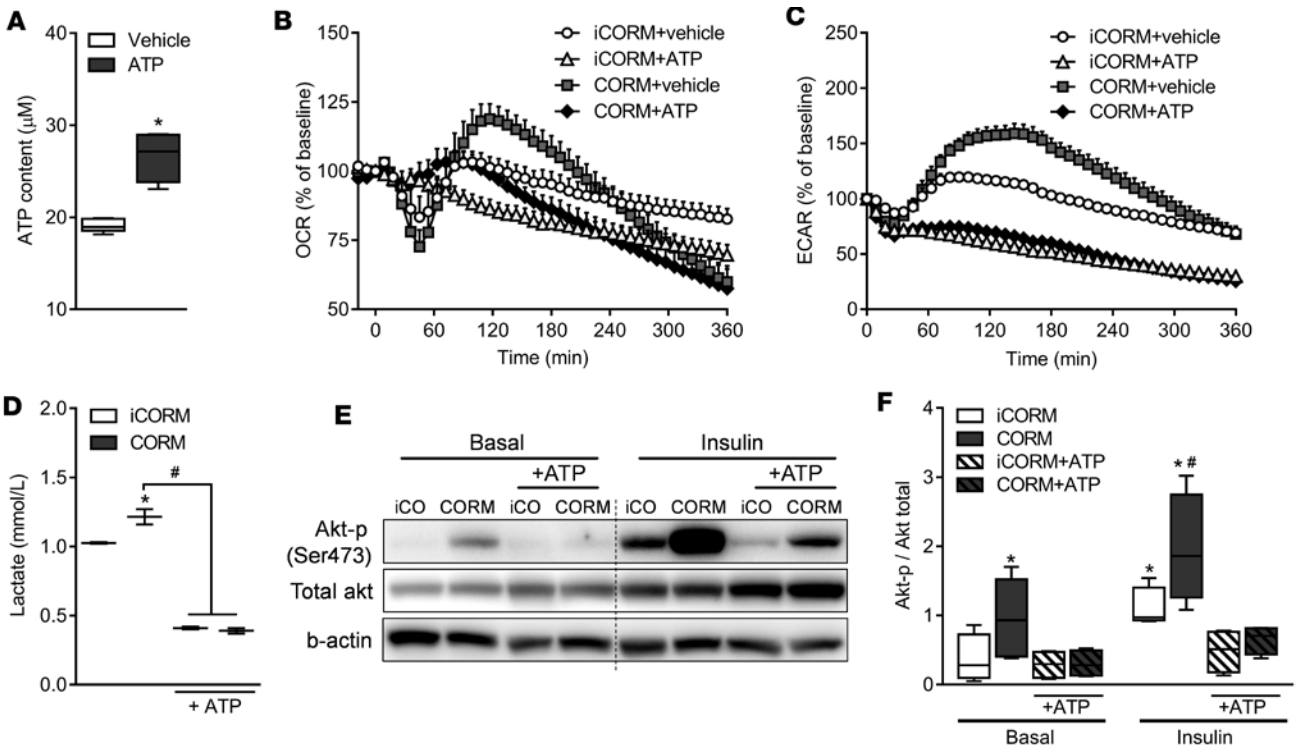

Figure 5. ATP counteracts CO induced–metabolic switch in adipocytes and reverses CO-induced increase in insulin sensitivity. Intracellular ATP (**A**) was measured after exposure of vehicle (H_2O) or ATP encapsulated in liposome. OCR (**B**) and ECAR (**C**) were measured for 6 hours after addition of iCORM (50 μM) or CORM-401 (50 μM) with or without vehicle (H_2O) or ATP encapsulated in liposome. Lactate content (**D**) after exposure of iCORM or CORM-401 with or without ATP. Expression of total Akt and phosphorylated Akt assessed by Western blot (**E** and **F**). Results are expressed as mean ± SEM. n = 3–4 independent experiments. *P < 0.05 vs. control group (CON), #P < 0.05 vs. insulin, Student's t test or 1-way ANOVA with Fisher multiple comparison test. Values not designated with symbols are not statistically different.

oxygen consumption and a decrease in ATP-linked respiration by CORM-401, which we attribute to an uncoupling activity by CO that we have demonstrated previously in isolated mitochondria as well as in endothelial and microglia cells (12, 15, 35–37). Thus, a potential defective ATP production in response to CO-mediated uncoupling would trigger glycolysis as a compensatory mechanism to preserve energy levels, leading to an improved systemic glucose profile. Indeed, ATP levels were maintained after CORM-401 treatment in adipocytes and were significantly decreased only in the presence of the glycolysis inhibitor 2-deoxyglucose. In addition, direct delivery of ATP into adipocytes prevented the metabolic switch (glycolysis and lactate production) and the increase in insulin sensitivity (Akt phosphorylation) without altering the uncoupling effect caused by CO. That is, when ATP is artificially raised in adipocytes, cells sense adequate energy levels and do not engage glycolysis, even though a diminished mitochondrial ATP production by the uncoupling activity of CO is still occurring. The increase in glycolysis exerted by CO in adipocytes is reminiscent of the action of metformin, an antidiabetic drug well known to improve insulin resistance in chronic obese patients (38) and capable of inhibiting mitochondrial ATP production (39). Notably, it has been reported that genetic alteration of mitochondrial oxidative phosphorylation improves insulin sensitivity in mice (6), while enhanced mitochondrial capacity in muscle is associated with higher risk of diabetes in humans (7). It is still debated whether mild increases or decreases in respiratory chain function are beneficial against insulin resistance. Our findings argue in favor of reducing respiratory chain function as a promising approach in the treatment of insulin resistance.

Uncoupling agents are renowned to promote weight loss because of their ability to dissipate energy as heat at the expense of ATP production by mitochondria (9, 40). Therefore, we propose that the transient uncoupling activity of CO elicited by repetitive administration of CORM-401 is a prominent mechanism responsible for the lower weight gain during the HFD regime. Because this uncoupling effect is concomitant to enhanced glycolysis, these two actions of CO appear to be essential in the restoration of metabolic homeostasis in obesity (Figure 6).

In summary, this study provides the first evidence to our knowledge that an orally active CO-releasing agent is effective in counteracting glucose intolerance and weight gain in HFD-fed obese mice. The ability of CO to interact with mitochondria and improve adipose tissue function seems to be central to this effect. Thus, our findings support the idea that CORM-401 could be investigated as a prototypic compound for the development of promising insulin-sensitizing agents.

Methods

Chemicals and reagents. CORM-401 (Mn(CO)4{S2CNMe(CH2CO2H)}) (see chemical structure in Supplemental Figure 1) was synthesized as previously described (41). Stock solutions (5–10 mM) were prepared by solubilizing CORM-401 in Dulbecco phosphate buffer solution (pH = 7.4) and stored at –20°C until use. As a negative control, CORM-401 was inactivated (iCORM) by incubation with equimolar concentrations of hydrogen peroxide for 24 hours in order to remove CO from CORM-401. The absence of CO release from iCORM was verified using a hemoglobin assay (see below). For the animal experiments, SD (A04) and HFD (Purified Diet 230 HF) were purchased from SAFE Diet. DMEM, penicillin/streptomycin, dexamethasone, newborn calf serum, and fetal bovine serum (FBS) were purchased from Life Technologies. Pyruvate, isobutylmethylxanthine (IBMX), insulin, and all other reagents were obtained from MilliporeSigma unless otherwise specified.

Animals and experimental design. Eight-week-old male C57BL6 mice weighing approximately 25 g were obtained from Janvier. Mice were housed under controlled conditions of temperature (21°C ± 1°C), hygrometry (60% ± 10%), and lighting (12 hours per day). Animals were acclimatized in the laboratory for 1 week before the start of the experiments. Mice were fed either a SD or a HFD for 14 weeks with or without CORM-401 treatment. In preliminary experiments, we tested CORM-401 at 15 mg/kg and 30 mg/kg, given orally 3 times a week, to evaluate its dose-dependent effects in our model. Because the effects were more pronounced with 30 mg/kg CORM-401, we continued our study using this dose and randomly divided mice into 5 groups (n = 10 per group): (a) SD-fed mice; (b) HFD-fed mice; (c) SD-fed mice administered CORM-401 starting at week 6 after the beginning of the diet (SD + CORM); (d) HFD-fed mice administered CORM-401 starting at week six after the beginning of the diet (treatment group, SD + CORM-T); and (e) HFD-fed mice administered with CORM-401 starting at the beginning of the diet (prevention group, SD + CORM-P). Mice were weighed weekly, and food consumption was measured at week 4 and 8. The total amount of food was weighed daily in the afternoon and averaged for each mouse to obtain a daily food consumption measurement per mouse. Mice were sacrificed at the end of 14 weeks after a 6-hour fast and 48 hours after the last CORM treatment. Blood was collected for biochemistry analysis and eWAT, inguinal white adipose tissue, BAT, and liver were removed and weighed. In an additional set of experiments, 6 hour–fasted mice were given PBS, iCORM (30 mg/kg), or CORM-401 (30 mg/kg) by oral gavage. Metabolic assays were performed 1 hour after CORM-401 administration for one set of experiment, and mice were sacrificed 2 hours after CORM-401 administration for experiments with the Seahorse Analyzer and adipose tissue collection.

Fasting blood glucose and glucose and insulin tolerance tests. After 6 hours of fasting, whole-body glucose tolerance and insulin sensitivity were assessed in all groups at weeks 5/6 and 12/13 by intraperitoneal glucose tolerance tests (GTTs) and insulin tolerance tests (ITTs), respectively. In addition, GTT and ITT were also evaluated 1 hour after oral gavage of CORM-401. First, blood was obtained via tail clip to assess fasting blood glucose (Caresens N, DinnoSante). Then, mice received a glucose (1.5 g/kg) or insulin (0.3 UI/kg) solution by intraperitoneal injection, and blood glucose was measured at 15, 30, 60, 90, and 120 minutes after the injection. The HOmeostasis Model Assessment of Insulin Resistance (HOMA-IR) adjusted to rodents was calculated as ([glucose (mg/dl)/18] × [insulin (ng/ml)/0.0347])/108.24, as reported previously (42) The area under the curve for the glucose excursion was calculated using Graphpad Prism.

Transthoracic echocardiography. Transthoracic echocardiography was performed in conscious mice as previously described (43, 44). Briefly, in hand-gripped mouse parasternal images were acquired at the level of papillary muscles using a 13-MHz linear-array transducer with a Vivid 7 ultrasound system (GE Medical System). Left ventricular dimensions were serially obtained in M-mode, and derived parameters were calculated using standard formulas. Left ventricular mass was determined using the uncorrected cube assumption (43, 44). Peak systolic values of strain rate in the anterior and posterior wall were obtained using Tissue Doppler Imaging. Strain rate analysis with EchoPac Software (GE Medical System) was performed offline by a blinded observer. Peak systolic strain rate on 8 consecutive cardiac cycles were averaged to reduce the effect of respiratory variations (43, 44).

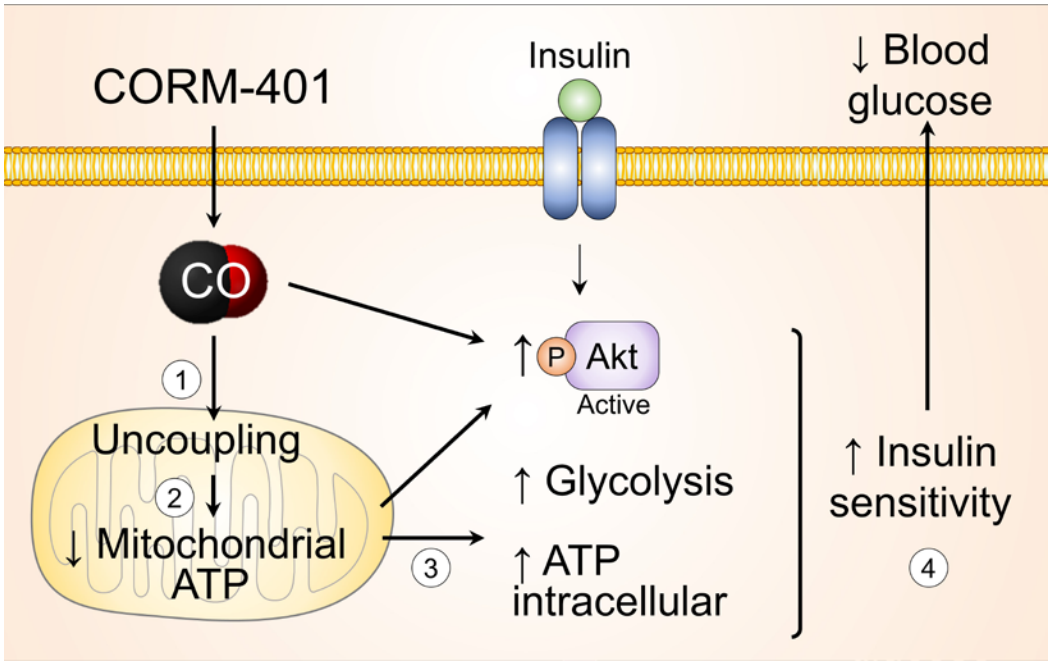

Figure 6. Proposed mechanism for the beneficial effects of CO on glucose metabolism in adipose tissue, leading to improvement in glucose homeostasis in obese mice. Obesity is characterized by adipose tissue dysfunction leading to insulin resistance and fasting hyperglycemia. CO delivered by CORM-401 in adipose tissue causes an uncoupling of mitochondrial respiration (noted as 1), resulting in a transient decrease in mitochondrial ATP production (noted as 2). As a counteracting mechanism to this effect, glycolysis is stimulated in cells, leading to maintenance to global intracellular ATP content (noted as 3). This metabolic switch in adipocytes improves local and systemic insulin sensitivity (noted as 4). A transient increase in adipose tissue insulin sensitivity resolves adipose tissue dysfunction as well as insulin resistance caused by obesity.

Preparation of eWAT-conditioned medium. eWAT (0.1 g) was collected and kept at room temperature in a 24-well plate with 1 ml DMEM/well. The tissue was minced into approximately 1-mm^3 pieces and incubated for 1 hours at 37°C and 5% CO_2 prior to transfer into a new plate with fresh DMEM medium containing 4.5 g glucose, 2 mM glutamine, 1% free fatty acid bovine serum albumin, and 1% antibiotic and antimycotic solution. eWAT-conditioned medium (eCM) was collected 24 hours after incubation and stored at –80°C until analysis.

Plasma and eCM analysis. An ELISA kit was used to measure insulin (ALPCO Diagnostics). Triglycerides, total cholesterol, lactate, alanine transaminase, aspartate transaminase, lactate dehydrogenase, and creatinine as well as conjugated and total bilirubin were measured in plasma samples using a Cobas 8000 analyzer (Roche). Cytokines (IL-1β, IL-10, and IL-6) and leptin were measured in plasma and eCM samples using Mesoscale Multiplex and Single-plex plates, respectively (Mesoscale Discovery).

Analysis of mRNA expression. After an initial extraction step by mixing Extract-All (Eurobio) and chloroform into samples, total RNA purification was performed with a column extraction Kit (RNeasy Mini, Qiagen). Double-strand cDNA was synthesized from total RNA with the High-Capacity cDNA Reverse Transcription Kit (Life Technologies). Quantitative real-time PCR was performed in a StepOnePlus Real-Time PCR System using commercially available TaqMan primer-probe sets (both from Life Technologies). Gene expression was assessed by the comparative CT (ΔΔCT) method, with β-actin as the reference gene.

Western blot analysis. Snap-frozen eWAT samples (200 mg) were lysed in cell lysis buffer (Cell Signaling, Danvers) supplemented with 1% phenylmethylsulfonyl fluoride. Protein samples were resolved on 12% bis-Tris gels followed by transfer to nitrocellulose membrane. Antibodies for Akt and phospho-Akt (Ser473) were from Cell Signaling (4991 and 4060, respectively), and antibodies for β-actin were from Santa Cruz (sc-47778). Bands were visualized by enhanced chemiluminescence and quantified using ImageJ software (NIH).

Histology and immunohistochemistry. Fresh tissues were fixed in 10% phosphate-buffered formalin overnight. Paraffin wax 5-μm sections were processed for H&E and CD68 immunostaining. Images were analyzed using ImageJ software.

3T3-L1 cell culture. 3T3-L1 murine preadipocytes (088SPL1F) were purchased from the ZenBio company and cultured in an atmosphere of 5% CO_2 at 37°C using DMEM supplemented with 10% newborn calf serum For adipocyte differentiation, cells were stimulated with 3T3-L1 differentiation medium containing IBMX (500 μM), dexamethasone (250 nM), and insulin (175 nM) for 2 days after cells reached confluency. The medium was changed to DMEM containing 10% FBS and insulin (175 nM) after 2 days, and adipocytes were then kept into DMEM containing only 10% FBS. Prior to the experiments, adipocytes were subjected to serum deprivation for 16 hours with DMEM supplemented with 0.5% FBS.

Cellular bioenergetic analysis. Bioenergetic profiles of 3T3-L1 adipocytes were determined using a Seahorse Bioscience XF24 Analyzer (Billerica) that provides real-time measurements of OCR, indicative of mitochondrial respiration, and ECAR, an index of glycolysis. An optimal cell density of 20,000 cells/well was determined from preliminary experiments. Bioenergetic measurements were performed in FBS- and bicarbonate-free DMEM (pH 7.4) supplemented with 4.5 g/l glucose, 1% glutamax, and 1% pyruvate to match the normal culture conditions of 3T3-L1 cells. In a first set of experiments, the effect of CORM-401 (25–100 μM) on OCR and ECAR was assessed over time. In a second set of experiments, the effect of CORM-401 on mitochondrial function was evaluated by means of a MitoStress test, which allows the measurements of key parameters such as ATP-linked respiration and proton leak after sequential additions of 1 μg/ml oligomycin (inhibitor of ATP synthesis), 0.7 μM carbonyl cyanide 4-(trifluoromethoxy) phenylhydrazone (FCCP, uncoupling agent), and 1 μM rotenone/antimycin A (inhibitors of complex I and complex III of the respiratory chain, respectively). CORM-401 was added 1 hour prior to oligomycin to ensure delivery of CO to cells before assessment of mitochondrial function. In an alternative set of experiments, we investigated the effect of CORM-401 on respiration in the absence of ATP synthesis by adding oligomycin to cells followed by CORM-401, FCCP, and rotenone/antimycin A. In a third set of experiments, the effect of CORM-401 on glycolysis was evaluated by means of a glycolytic stress test, which allow the measurements of glycolysis and glycolytic reserve capacity after sequential additions of 10 mM glucose, 1 μg/ml oligomycin, and 50 mM of 2-deoxyglucose (inhibitor of glycolysis). The pharmacological action of CORM-401 was compared with that of iCORM-401, which does not release CO.

ATP assay. Intracellular ATP levels were measured using an ATPLite Bioluminescence Assay Kit (PerkinElmer) according to the manufacturer's instructions.

Assays for the detection of CO in vivo and in vitro. The levels of COHb in blood were determined as previously described by our group (45). Briefly, blood (5 μl) collected from the mouse tail vein at different time points after oral administration with CORM-401 was added to a cuvette containing 4.5 ml deoxygenated tris(hydroxymethyl) aminomethane solution, and spectra were recorded as reported above. The percentage of COHb was calculated based on the absorbance at 420 and 432 nm, with the reported extinction coefficients for mouse blood (46). The detection of CO content in adipose tissue following oral gavage with CORM-401 was determined using the method of Vreman et al. (47). For this, adipose tissues were initially placed in ice-cold potassium phosphate buffer (1:4 w/v) and stored at –80°C until analysis. The day of the experiment, tissues were diced and sonicated and 40 μl of this suspension was added to CO-free sealed vials containing 5 ml of 30% (w/v) sulfosalicylic acid and incubated for 30 minutes on ice. CO released into the vial headspace was quantified by gas chromatography. CO accumulated in cultured 3T3-L1 adipocytes after treatment with CORM-401 was measured spectrophotometrically using a specific scavenger of CO (hemoCD1) as previously described (48).

Statistics. Data are expressed as mean values ± SEM. Statistical analyses were performed using the unpaired 2-tailed Student's *t* test or 1-way or 2-way ANOVA with Fisher multiple comparison test. The result was considered significant if the *P* value was less than 0.05.

Study approval. All animals received care according to the institutional guidelines of Inserm, and all experiments were approved by Institutional Ethics Committee number 16, Paris, France (licence 16-090).

Author contributions

LB, RF, and RM designed the study, performed experiments, collected and analyzed data, and wrote the manuscript. LB and MP performed metabolic tests. LM performed CO measurements in adipose tissue. SM performed histological staining. HK provided critical materials and advice on the use of hemoCD1. LB, MP, DS, and GC collected organs for analysis. JT performed the echocardiography. GD analyzed the echocardiography and read the manuscript. RM is the guarantor of this work and, as such, had full access to all the data in this study and takes responsibility for the integrity of the data and the accuracy of the data analysis.

Acknowledgments

This work was supported by a grant from the French National Research Agency (ANR) (ANR-15-RHUS-0003). The authors thank Jayne Louise Wilson for her support in teaching the use of the Seahorse Analyzer. The authors also thank Rachid Souktani and Cécile Lecointe for help in the animal facility platform; Xavier Decrouy, Christelle Gandolphe, and Wilfried Verbecq-Morlot from the histology platform; and Stéphane Moutereau at Henri Mondor Hospital for blood analysis.

Address correspondence to: Roberto Motterlini or Roberta Foresti, Inserm U955, Team 12, Faculty of Medicine, University Paris-Est, 24 rue du Général Sarrail, 94000 Créteil. Phone: 33.149813637. Email: roberto.motterlini@inserm.fr (R. Motterlini); roberta.foresti@inserm.fr (R. Foresti).

1. Stumvoll M, Goldstein BJ, van Haeften TW. Type 2 diabetes: principles of pathogenesis and therapy. *Lancet*. 2005;365(9467):1333–1346.
2. Guilherme A, Virbasius JV, Puri V, Czech MP. Adipocyte dysfunctions linking obesity to insulin resistance and type 2 diabetes. *Nat Rev Mol Cell Biol*. 2008;9(5):367–377.
3. Barazzoni R, Gortan Cappellari G, Ragni M, Nisoli E. Insulin resistance in obesity: an overview of fundamental alterations. *Eat Weight Disord*. 2018;23(2):149–157.
4. Montgomery MK, Turner N. Mitochondrial dysfunction and insulin resistance: an update. *Endocr Connect*. 2015;4(1):R1–R15.
5. Fazakerley DJ, et al. Mitochondrial oxidative stress causes insulin resistance without disrupting oxidative phosphorylation. *J Biol Chem*. 2018;293(19):7315–7328.
6. Pospisilik JA, et al. Targeted deletion of AIF decreases mitochondrial oxidative phosphorylation and protects from obesity and diabetes. *Cell*. 2007;131(3):476–491.
7. Nair KS, et al. Asian Indians have enhanced skeletal muscle mitochondrial capacity to produce ATP in association with severe insulin resistance. *Diabetes*. 2008;57(5):1166–1175.
8. Green K, Brand MD, Murphy MP. Prevention of mitochondrial oxidative damage as a therapeutic strategy in diabetes. *Diabetes*. 2004;53 Suppl 1:S110–S118.
9. Harper JA, Dickinson K, Brand MD. Mitochondrial uncoupling as a target for drug development for the treatment of obesity. *Obes Rev*. 2001;2(4):255–265.
10. Tao H, Zhang Y, Zeng X, Shulman GI, Jin S. Niclosamide ethanolamine-induced mild mitochondrial uncoupling improves diabetic symptoms in mice. *Nat Med*. 2014;20(11):1263–1269.
11. Crunkhorn S. Metabolic disease: Mitochondrial uncoupler reverses diabetes. *Nat Rev Drug Discov*. 2014;13(12):885.
12. Wilson JL, et al. Carbon monoxide reverses the metabolic adaptation of microglia cells to an inflammatory stimulus. *Free Radic Biol Med*. 2017;104:311–323.
13. Lavitrano M, et al. Carbon monoxide improves cardiac energetics and safeguards the heart during reperfusion after cardiopulmonary bypass in pigs. *FASEB J*. 2004;18(10):1093–1095.
14. Almeida AS, Sonnewald U, Alves PM, Vieira HL. Carbon monoxide improves neuronal differentiation and yield by increasing the functioning and number of mitochondria. *J Neurochem*. 2016;138(3):423–435.
15. Motterlini R, Foresti R. Biological signaling by carbon monoxide and carbon monoxide-releasing molecules. *Am J Physiol, Cell Physiol*. 2017;312(3):C302–C313.
16. Motterlini R, Foresti R. Heme oxygenase-1 as a target for drug discovery. *Antioxid Redox Signal*. 2014;20(11):1810–1826.
17. Motterlini R, Otterbein LE. The therapeutic potential of carbon monoxide. *Nat Rev Drug Discov*. 2010;9(9):728–743.
18. Foresti R, Braud L, Motterlini R. Signaling and Cellular Functions of Carbon Monoxide (CO). In: Wang R, ed. *Metallobiology Series - Gasotransmitters*. Cambridge, UK: RSC Publishing; 2018:161–191.
19. Clark JE, et al. Cardioprotective actions by a water-soluble carbon monoxide-releasing molecule. *Circ Res*. 2003;93(2):e2–e8.
20. Fayad-Kobeissi S, et al. Vascular and angiogenic activities of CORM-401, an oxidant-sensitive CO-releasing molecule. *Biochem Pharmacol*. 2016;102:64–77.
21. Hosick PA, et al. Chronic carbon monoxide treatment attenuates development of obesity and remodels adipocytes in mice fed a high-fat diet. *Int J Obes (Lond)*. 2014;38(1):132–139.
22. Hosick PA, AlAmodi AA, Hankins MW, Stec DE. Chronic treatment with a carbon monoxide releasing molecule reverses dietary induced obesity in mice. *Adipocyte*. 2016;5(1):1–10.
23. Wegiel B, et al. Carbon monoxide expedites metabolic exhaustion to inhibit tumor growth. *Cancer Res*. 2013;73(23):7009–7021.
24. Cai D, et al. Local and systemic insulin resistance resulting from hepatic activation of IKK-beta and NF-kappaB. *Nat Med*. 2005;11(2):183–190.
25. Kim HJ, et al. Differential effects of interleukin-6 and -10 on skeletal muscle and liver insulin action in vivo. *Diabetes*. 2004;53(4):1060–1067.
26. Jais A, et al. Heme oxygenase-1 drives metaflammation and insulin resistance in mouse and man. *Cell*. 2014;158(1):25–40.
27. Li M, et al. Treatment of obese diabetic mice with a heme oxygenase inducer reduces visceral and subcutaneous adiposity, increases adiponectin levels, and improves insulin sensitivity and glucose tolerance. *Diabetes*. 2008;57(6):1526–1535.
28. Ndisang JF, Lane N, Jadhav A. Upregulation of the heme oxygenase system ameliorates postprandial and fasting hyperglycemia in type 2 diabetes. *Am J Physiol Endocrinol Metab*. 2009;296(5):E1029–E1041.
29. Nicolai A, et al. Heme oxygenase-1 induction remodels adipose tissue and improves insulin sensitivity in obesity-induced diabetic rats. *Hypertension*. 2009;53(3):508–515.
30. Burgess A, et al. Adipocyte heme oxygenase-1 induction attenuates metabolic syndrome in both male and female obese mice. *Hypertension*. 2010;56(6):1124–1130.

31. Huang JY, Chiang MT, Yet SF, Chau LY. Myeloid heme oxygenase-1 haploinsufficiency reduces high fat diet-induced insulin resistance by affecting adipose macrophage infiltration in mice. *PLoS ONE*. 2012;7(6):e38626.
32. Kim HJ, et al. Carbon monoxide protects against hepatic ischemia/reperfusion injury via ROS-dependent Akt signaling and inhibition of glycogen synthase kinase 3β. *Oxid Med Cell Longev*. 2013;2013:306421.
33. Yang PM, Huang YT, Zhang YQ, Hsieh CW, Wung BS. Carbon monoxide releasing molecule induces endothelial nitric oxide synthase activation through a calcium and phosphatidylinositol 3-kinase/Akt mechanism. *Vascul Pharmacol*. 2016;87:209–218.
34. Wegiel B, et al. Nitric oxide-dependent bone marrow progenitor mobilization by carbon monoxide enhances endothelial repair after vascular injury. *Circulation*. 2010;121(4):537–548.
35. Lo Iacono L, et al. A carbon monoxide-releasing molecule (CORM-3) uncouples mitochondrial respiration and modulates the production of reactive oxygen species. *Free Radic Biol Med*. 2011;50(11):1556–1564.
36. Kaczara P, et al. Carbon monoxide released by CORM-401 uncouples mitochondrial respiration and inhibits glycolysis in endothelial cells: A role for mitoBKCa channels. *Biochim Biophys Acta*. 2015;1847(10):1297–1309.
37. Sandouka A, et al. Carbon monoxide-releasing molecules (CO-RMs) modulate respiration in isolated mitochondria. *Cell Mol Biol (Noisy-le-grand)*. 2005;51(4):425–432.
38. González-Barroso MM, Anedda A, Gallardo-Vara E, Redondo-Horcajo M, Rodríguez-Sánchez L, Rial E. Fatty acids revert the inhibition of respiration caused by the antidiabetic drug metformin to facilitate their mitochondrial β-oxidation. *Biochim Biophys Acta*. 2012;1817(10):1768–1775.
39. Zhang Y, Ye J. Mitochondrial inhibitor as a new class of insulin sensitizer. *Acta Pharm Sin B*. 2012;2(4):341–349.
40. Speakman JR, et al. Uncoupled and surviving: individual mice with high metabolism have greater mitochondrial uncoupling and live longer. *Aging Cell*. 2004;3(3):87–95.
41. Crook SH, et al. [Mn(CO)4{S2CNMe(CH2CO2H)}], a new water-soluble CO-releasing molecule. *Dalton Trans*. 2011;40(16):4230–4235.
42. Lee S, et al. Comparison between surrogate indexes of insulin sensitivity and resistance and hyperinsulinemic euglycemic clamp estimates in mice. *Am J Physiol Endocrinol Metab*. 2008;294(2):E261–E270.
43. Sawaki D, et al. Visceral adipose tissue drives cardiac aging through modulation of fibroblast senescence by osteopontin production. *Circulation*. 2018;138(8):809–822.
44. Ternacle J, et al. Short-term high-fat diet compromises myocardial function: a radial strain rate imaging study. *Eur Heart J Cardiovasc Imaging*. 2017;18(11):1283–1291.
45. Nikam A, et al. Diverse Nrf2 activators coordinated to cobalt carbonyls induce heme oxygenase-1 and release carbon monoxide in vitro and in vivo. *J Med Chem*. 2016;59(2):756–762.
46. Rodkey FL, Hill TA, Pitts LL, Robertson RF. Spectrophotometric measurement of carboxyhemoglobin and methemoglobin in blood. *Clin Chem*. 1979;25(8):1388–1393.
47. Vreman HJ, Wong RJ, Kadotani T, Stevenson DK. Determination of carbon monoxide (CO) in rodent tissue: effect of heme administration and environmental CO exposure. *Anal Biochem*. 2005;341(2):280–289.
48. Minegishi S, et al. Detection and removal of endogenous carbon monoxide by selective and cell-permeable hemoprotein model complexes. *J Am Chem Soc*. 2017;139(16):5984–5991.